Mechanosynthesis and Thermoelectric Properties of Fe, Zn, and Cd-Doped P-Type Tetrahedrite: $Cu_{12-x}M_xSb_4S_{13}$

Francisco Arturo López Cota [1,*], José Alonso Díaz-Guillén [2], Oscar Juan Dura [3], Marco Antonio López de la Torre [3], Joelis Rodríguez-Hernández [4] and Antonio Fernández Fuentes [1,*]

1   Cinvestav Unidad Saltillo, Apartado Postal 663, Saltillo 25000, Coahuila, Mexico
2   División de Estudios de Posgrado e Investigación, Instituto Tecnológico de Saltillo, Saltillo 25280, Coahuila, Mexico; j.a.diazguillen@gmail.com
3   GFMA, Departamento de Física Aplicada, Escuela Técnica Superior de Ingenieros Industriales, Universidad de Castilla-La Mancha, 13071 Ciudad Real, Spain; oscar.juan@uclm.es (O.J.D.); marcoantonio.lopez@uclm.es (M.A.L.d.l.T.)
4   Centro de Investigación en Química Aplicada, Saltillo 25294, Coahuila, Mexico; joelis.rodriguez@ciqa.edu.mx
*   Correspondence: f.a.lopez.cota@gmail.com (F.A.L.C.); antonio.fernandez@cinvestav.edu.mx (A.F.F.); Tel.: +52-8442924211 (F.A.L.C.); +52-8444389600 (A.F.F.)

Abstract: This contribution deals with the mechanochemical synthesis, characterization, and thermoelectric properties of tetrahedrite-based materials, $Cu_{12-x}M_xSb_4S_{13}$ (M = Fe^{2+}, Zn^{2+}, Cd^{2+}; x = 0, 1.5, 2). High-energy mechanical milling allows obtaining pristine and substituted tetrahedrites, after short milling under ambient conditions, of stoichiometric mixtures of the corresponding commercially available binary sulfides, i.e., Cu_2S, CuS, Sb_2S_3, and MS (M = Fe^{2+}, Zn^{2+}, Cd^{2+}). All the target materials but those containing Cd were obtained as single-phase products; some admixture of a hydrated cadmium sulfate was also identified by XRD as a by-product when synthesizing $Cu_{10}Cd_2Sb_4S_{13}$. The as-obtained products were thermally stable when firing in argon up to a temperature of 350–400 °C. Overall, the substitution of Cu(II) by Fe(II), Zn(II), or Cd(II) reduces tetrahedrites' thermal and electrical conductivities but increases the Seebeck coefficient. Unfortunately, the values of the thermoelectric figure of merit obtained in this study are in general lower than those found in the literature for similar samples obtained by other powder processing methods; slight compositional changes, undetected secondary phases, and/or deficient sintering might account for some of these discrepancies.

Keywords: thermoelectric; mechanosynthesis; tetrahedrites; Seebeck; thermal conductivity; figure of merit; electrical conductivity

1. Introduction

Thermoelectric materials have gained in recent years special relevance in multiple energy-related applications, such as power generation or waste heat recovery [1,2]. Using the Seebeck effect, thermoelectric materials convert a temperature gradient into a voltage difference and thereby transform thermal energy directly into electricity (and vice versa). Their efficiency is assessed by a dimensionless quantity known as the thermoelectric figure of merit, which is represented by (zT) and given by the mathematical expression (zT) = $\sigma S^2 T/\kappa$, where S is the Seebeck coefficient, σ represents the electrical conductivity, T is the absolute temperature and κ is the thermal conductivity. Moreover, the ideal thermoelectric material (high (zT) values) would be one having a high electrical conductivity and Seebeck coefficient but low thermal conductivity [3]; unfortunately, finding candidate materials meeting these criteria has proven very difficult because the three (S, σ, and κ) are coupled, and any attempt to optimize one affects the remaining two.

Commonly available thermoelectric materials at present include Bi_2Te_3, PbTe-based materials, and Si-Ge alloys; however, increasing concerns about the cost, long-term availability, and environmental impact of some of their constituent chemical elements have

fueled the search for more benign alternatives [4,5]. Among them, $Cu_{12}Sb_4S_{13}$-based tetrahedrites have been identified as a very promising group of low-cost and environmentally friendly thermoelectric materials. This mixed valence Cu^+/Cu^{2+} sulfide features an isometric unit cell (Space Group $I\bar{4}3m$ (#217)) with a single Sb site, two equally populated Cu sites, and two S positions in a rather complex crystal structure with a large number of atoms per unit cell (Z = 2); furthermore, tetrahedrites can accommodate a large variety of Cu and Sb substitutions, display p-type semiconducting behavior, and have intrinsically low thermal conductivity, which are all desirable characteristics for a thermoelectric material. Their ample chemical and structural flexibility allow for the tuning of their properties for different energy-related applications such as supercapacitors, photovoltaics, or catalysis, to mention some [6–9]. Herein, we describe a simple solid-state method to prepare pure and substituted tetrahedrites $Cu_{12-x}M_xSb_4S_{13}$ (M = Cd, Zn and Fe), using binary sulfides as starting materials. Metal sulfides are generally prepared in laboratory, by firing either under vacuum or in oxygen-free environments, stoichiometric powdered mixtures of high-purity sulfur and the corresponding metal(s) or by complex and lengthy solution-mediated methods [10–12]. Alternatively, they have been also obtained from the elements by dry or liquid-assisted mechanochemical methods under controlled atmospheres, or through a mechanically induced chemical reaction between an alkali metal sulfide and the corresponding metal acetates [13–16]. The synthesis of tetrahedrite-based mixed sulfides by reacting volatile sulfur (b.p. = 717.8 K) and high melting point Cu (m.p. = 1357.8 K) is particularly complex, and it must be carried out in evacuated and sealed glass ampoules to minimize sulfur losses and ensure single-phase products with controlled stoichiometries. Furthermore, the synthesis is hindered by the difficulties in controlling the final oxidation state of copper, which should be present as mixed Cu(I)/Cu(II). This article describes an alternative method for obtaining tetrahedrites from commercially available binary sulfides, using high-energy mechanical milling under ambient conditions. Mechanochemically obtained materials are frequently highly defective and metastable phases, featuring a large variety of structural defects such as vacancies, antisite defects, and dislocations [17]. Defects might be beneficial for suppressing the materials' thermal conductivity and thus for increasing the thermoelectric figure of merit [18]. The proposed methodology might be a feasible high-throughput route for producing different complex chalcogenides, even using naturally occurring and relatively abundant sulfide minerals, as starting chemicals.

2. Materials and Methods

The synthesis of the title materials was carried out by high-energy mechanical milling, using commercially available binary sulfides (i.e., Cu_2S, CuS, Sb_2S_3, FeS, ZnS, and CdS) as starting chemicals. As-received reactants (Sigma-Aldrich Inc., St. Louis, MO, USA, ≥99%) were weighed out as required by stoichiometry to obtain the corresponding $Cu_{12-x}M_xSb_4S_{13}$ (M = Cd, Zn, and Fe) materials and then hand mixed in an agate mortar and placed in 125 mL YPSZ containers (5 mol% Y_2O_3) together with 20 mm diameter YPSZ balls as grinding media (ball/powder mass ratio = 10:1). Milling was performed under ambient conditions (air) in a Retsch PM400 planetary mill (Retsch GmbH, Haan, Germany), using a rotating sun-wheel speed of 350 rpm (vial-to-wheel speed ratio 1:−2). The evolution of the reacting mixtures with milling time was followed by sampling the content of the jar at different time intervals (30 min, 1, 3, and 6 h), and analyzing the as-obtained powders by X-ray diffraction (XRD) (Rigaku Ultima IV, Rigaku Co, Tokyo, Japan). All mechanically induced chemical reactions were considered completed when no traces of the starting powders were identified by this technique.

Characterization

For the structural analysis, XRD patterns were collected at room temperature using CuKα radiation (typical scan rate = 2° min^{-1}, in 0.02° (2θ) steps) and a Rigaku Ultima IV diffractometer equipped with a D/teX detector. Structural refinement of the XRD data was performed by using the Rietveld method, implemented in the FULLPROF program [19].

Cell parameters and peak profiles were refined using Le Bail's pattern fitting method and a pseudo-Voigt peak shape function [20], whereas the background was modeled by a third-order polynomial fitting. Reference structural data for tetrahedrite were obtained from the Inorganic Crystal Structure Database [21]. The thermal stability of the as-obtained powders was analyzed by recording simultaneously their weight change and heat flow (TGA/DTA) between room temperature and 550 °C using a TA Instruments SDT 600 Analyzer (TA Instruments, New Castle, DE, USA) (typical sample size 5 mg; flowing argon = 100 mL/min; heating rate = 10 °C/min).

Thermal properties were analyzed in pellets ($\approx$0.5 cm thickness and 1.3 cm diameter) prepared by uniaxially pressing (5 ton/cm^2) and firing (350 °C; soaking time = 1 h) the mechanochemically obtained mixed sulfides. Thermal diffusivities (α) were determined by the laser pulse technique (inert atmosphere), with a commercial LINSEIS LFA 1000 equipment (Linseis Messgeräte GmbH, Selb, Germany). Before every measurement, samples were coated with a thin layer of colloidal graphite to ensure full absorption of the energy pulse at the pellet's front side and the highest emissivity from the back side. Samples and coating stability were confirmed by performing three consecutive analyses under identical conditions. Heat capacity was determined with the help of a simultaneous DSC/TGA Jupiter Netzsch STA 449C equipment (Netzsch Holding, Selb, Germany) in the temperature range from 50 to 350 °C (Pt crucibles; heating rate = 10 °C/min; an argon flow = 35 mL/min). A sapphire single crystal sample was used as reference material. As before, several runs were carried out for each sample to verify our experimental data reproducibility and accuracy.

The Seebeck coefficient was measured in the temperature range from 50 to 350 °C (under vacuum; heating rate = 5 °C/min) in an MMR-Technologies SB-100 instrument (MMR Technologies Inc, Mountain View, CA, USA), taking three readings every 25 °C. Resistivity measurements were made at the same conditions as the Seebeck coefficient, using a Keithley 2400 Source Meter (Tektronix Inc, Beaverton, OR, USA).

3. Results and Discussion

3.1. X-ray Diffraction (XRD)

Figure 1a shows a comparison between the XRD patterns collected for the as-obtained $Cu_{12}Sb_4S_{13}$ and $Cu_{12-x}M_xSb_4S_{13}$ samples (x = 1.5, 2; M = Fe^{2+}, Cd^{2+}, and Zn^{2+}), after milling the corresponding reacting mixtures for 6 h, as described in the previous section. All reacting mixtures present after this milling time an XRD pattern similar to that described in the literature as characteristic of cubic tetrahedrite. Accordingly, the numbers in parentheses in Figure 1a are the corresponding Miller indexes, as stated in ICSD #84571. The purity and room-temperature crystallographic characteristics of the as-prepared sulfides were analyzed by XRD using the Rietveld method and the corresponding crystal data from the literature. Figure 1b shows the graphic result of the refinement carried out in the $Cu_{10}Cd_2Sb_4S_{13}$ sample, whereas Table 1 presents the results and reliability factors for the whole series. Fe and Zn-containing mixtures produced single-phase products, whereas the XRD pattern collected for the sample with the highest Cd content ($Cu_{10}Cd_2Sb_4S_{13}$) showed in Figure 1b also contains two additional and very low intensity reflections at 18 and 25° (2θ). These reflections suggest the existence of a small admixture of $CdSO_4 \cdot H_2O$ as secondary phase. The crystal chemistry of copper-based sulfides is rather complex and determined to a great extent by the S/Cu atomic ratio [22]. Thus, all Cu atoms are found in almost regular tetrahedral coordination when Cu/S << 1, but in irregular geometries with lower coordination numbers, when the ratio is close to or greater than 1. In tetrahedrite (Cu/S = 0.92), half of all Cu atoms occupy the Wyckoff 12d tetrahedral site (coordination polyhedra CuS_4), and the other half sits at the Wyckoff 12e site, adopting a rather unusual trigonal planar coordination (coordination polyhedra CuS_3); substituting divalent metals replacing Cu are limited to two atoms per formula unit ($0 \leq x \leq 2$) and occupy preferentially the tetrahedral site. According to the results summarized in Table 1, all the samples prepared in this work were successfully refined using the tetrahedrite crystal

structure [16,23]. Depending on the substituent element, our results show that they have cell parameters ranging from 10.366 to 10.462 Å, similar to those reported in the literature for partially substituted tetrahedrites [24,25]. The largest change, which is evidenced in the diffraction pattern with a small shift toward higher angles (2θ), corresponds to the tetrahedrite where 100% of CuS was replaced by CdS; this change is mostly due to the ionic radius of cadmium, which shows the largest mismatch to that of Cu.
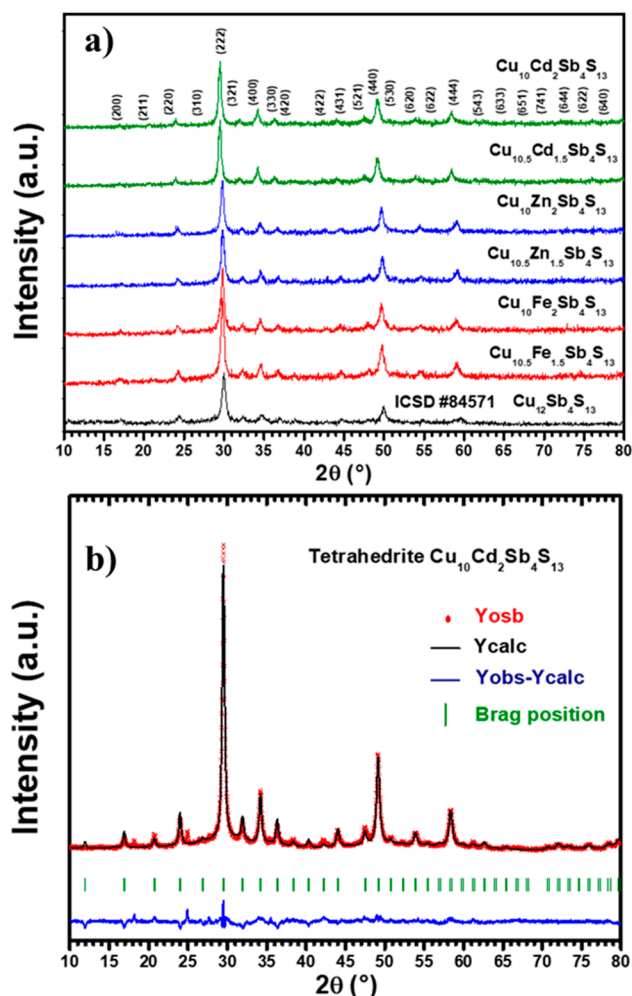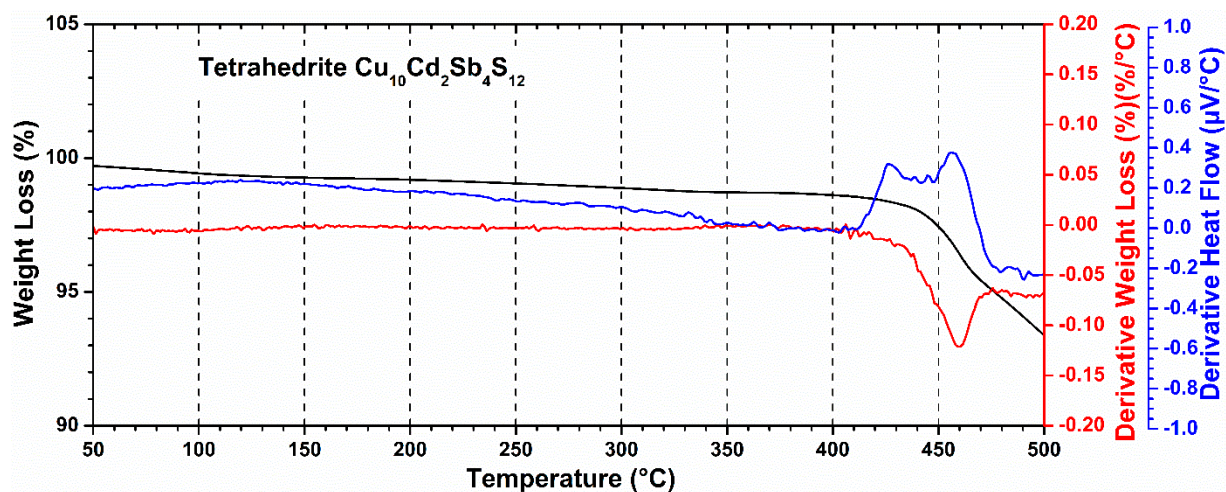

Figure 1. (**a**) XRD patterns for $Cu_{12-x}M_xSb_4S_{13}$ (x = 1.5, 2) compared with the standard data ICSD #84571. (**b**) Rietveld refinement graph of $Cu_{10}Cd_2Sb4S_{13}$.

3.2. Thermal Analysis

A series of thermal analysis studies were carried out to identify the thermal stability of these materials, which is important when determining their maximum operating temperature. In Figure 2, it is possible to observe the percentage of weight loss, the derivative weight loss, and the derivative heat flow for the reference sample $Cu_{10}Cd_2Sb_4S_{13}$, which was selected as representative for the series. The material obtained presents thermal stability until 400 °C, determining this as the operating range. The maximum weight loss of the composition starts at a temperature of 460 °C, which is probably due to sulfur loss. However, it was decided to measure the electrical and thermal properties in a range of 50 to 350 °C, since the rest of the phases decomposed at lower temperatures.

Table 1. Experimental details for the XRD data recording and processing.

Compound	$Cu_{10.5}Cd_{1.5}Sb_4S_{13}$	$Cu_{10}Cd_2Sb_4S_{13}$	$Cu_{10.5}Zn_{1.5}Sb_4S_{13}$	$Cu_{10}Zn_2Sb_4S_{13}$	$Cu_{10.5}Fe_{1.5}Sb_4S_{13}$	$Cu_{10}Fe_2Sb_4S_{13}$
ICSD			845	71		
Unit Cell						
Space group	I-43m	I-43m	I-43m	I-43m	I-43m	I-43m
Cell parameters (Å)	a = 10.4627(10)	a = 10.4870(9)	a = 10.3540(9)	a = 10.3667(9)	a = 10.3562(13)	a = 10.3662(12)
V(Å^3)	1145.33(2)	1153.33(2)	1110.01(2)	1114.09(2)	1110.71(2)	1113.93(2)
Z	2	2	2	2	2	2
Refinement						
Number of reflections	51	51	51	51	51	51
Number of refined parameters						
Structural	9	9	9	9	9	9
Profile	8	8	8	8	8	8
Rexp	1.85	1.87	1.88	1.9	1.86	1.96
Rwp	3.98	3.81	3.84	3.92	3.68	3.7
R_B	2.33	2.26	2.22	2.23	2.1	2.13
S	2.15	2.04	2.04	2.06	1.97	1.89

Figure 2. Weight loss, derivative weight loss, and derivative of DTA for phase $Cu_{10}Cd_2Sb4S_{13}$.
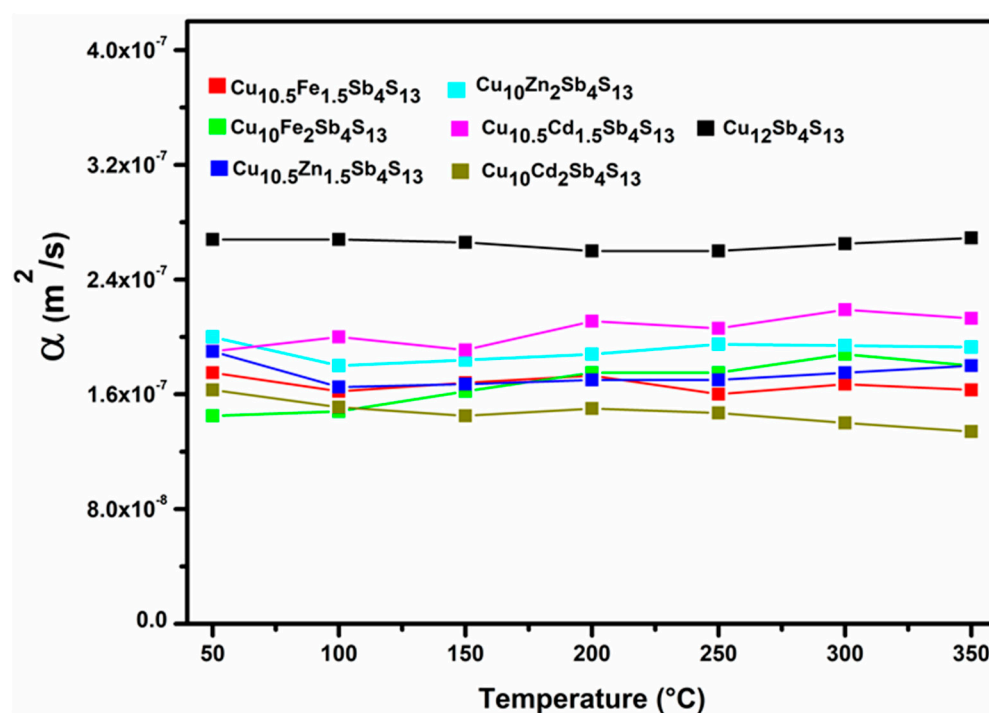
3.3. Thermal Conductivity

To determine the thermal properties of the material, it was necessary to measure each of the components that make up the figure of merit. The first to be measured was the Cp inherent in the samples studied; Table 2 shows the heat capacity of the different phases studied at a temperature of 350 °C. Likewise, the phase tetrahedrite without substitution was used as a reference. From the table, it is appreciated that all the phases present similar Cp values.

Figure 3 shows the thermal diffusivity of each phase studied. It is evident that the unsubstituted tetrahedrite has a higher thermal diffusivity (2.69×10^{-7} m^2/s) than the remaining tetrahedrites. Of the mono-substituted compounds, the one with the highest diffusivity values is the sample $Cu_{10.5}Cd_{1.5}Sb_4S_{13}$ with 2.13×10^{-7} m^2/s, while the one with the lowest levels is the sample $Cu_{10}Cd_2Sb_4S_{13}$ 1.34×10^{-7} m^2/s.

Table 2. Heat capacity for mono-substituted tetrahedrites at 350 °C.

	Tetrahedrites	Cp J/kg K
Pristine	$Cu_{12}Sb_4S_{13}$	515.99
Mono-substituted	$Cu_{10.5}Fe_{1.5}Sb_4S_{13}$	524.29
	$Cu_{10}Fe_2Sb_4S_{13}$	567.043
	$Cu_{10.5}Zn_{1.5}Sb_4S_{13}$	548.63
	$Cu_{10}Zn_2Sb_4S_{13}$	522.67
	$Cu_{10.5}Cd_{1.5}Sb_4S_{13}$	559.22
	$Cu_{10}Cd_2Sb_4S_{13}$	495.12

Figure 3. Behavior of thermal diffusivity for the unsubstituted tetrahedrite phase and for the mono-substituted tetrahedrites, in a temperature range between 50 and 350 °C.

The thermal conductivity for each of the mono-substituted samples as well as that of the unsubstituted tetrahedrite are presented in Figure 4; the sample that presents the highest thermal conductivity is the tetrahedrite without substitution (0.65 W/m K), while the rest of the samples present lower levels of conductivity between 0.35 and 0.5 W/m K. The heat capacity is similar for all these materials, as well as their density, since they have the same chemical base only with small variations, being the thermal diffusivity the one that implies a drastic change at the moment of obtaining the thermal conductivity of the material. The total thermal conductivity has two major contributions: the lattice part, which accounts for the propagation of phonons through the crystalline lattice, and the electronic part (κ_e) accounting for the transport of heat with charger carriers. The electronic part of the thermal conductivity was calculated using the Wiedemann–Franz law as $\kappa_e = L_0\sigma T$, where L_0 is the ideal Lorenz number, 2.44×10^{-8} WΩK^{-2}, σ is the electrical conductivity, and T is the absolute temperature. The electronic part of the thermal conductivity is very low and accounts for no more than 1% of the total thermal conductivity [26]. The decrease in thermal conductivity for the mono-substituted samples may be due to point defects generated with the incorporation of substituents to the crystal lattice or to dislocations produced during the mechanical grinding of the material.
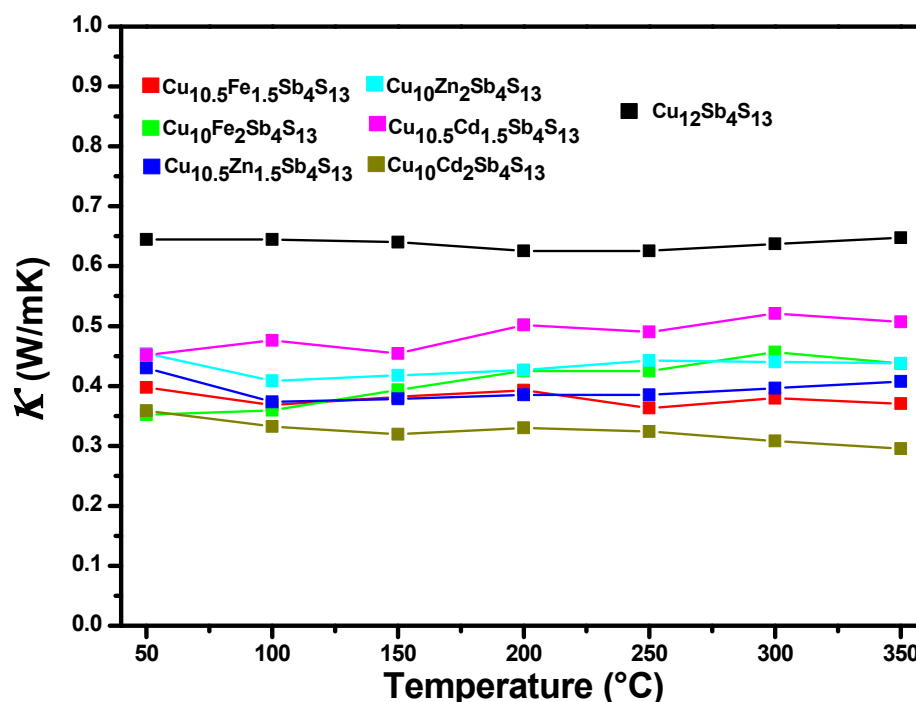
Figure 4. Behavior of thermal conductivity for the tetrahedrite phase without substitution and for the mono-substituted tetrahedrites.

3.4. Power Factor

The first element analyzed that integrates the power factor into the figure of merit is the Seebeck coefficient, which can be observed in Figure 5 for each studied sample. The highest values obtained for the Seebeck coefficient correspond to the compound $Cu_{10.5}Fe_{1.5}Sb_4S_{13}$, while tetrahedrite without substitution was the sample with the lowest coefficient in almost every single temperature. Every single result is similar or even higher than those reported [27]. Most of the compounds show a general behavior of between 130 and 272 µV/K. The results of this measurement agree even with tetrahedrites of mineral origin, which indicates a similarity of the synthetic phase with the natural tetrahedrite [28]. The positive behavior in the Seebeck coefficient indicates that they are p-type semiconductors indicating that majority carriers are holes, forming a network that will allow an electronic flow through it.

The electrical conductivity that is inverse to the resistivity was analyzed for each compound and can be seen in Figure 6. Tetrahedrite in its base form is the one with the highest conductivity value with 1877 S/m, while the samples corresponding to the $Cu_{10.5}Fe_{1.5}Sb4S_{13}$, $Cu_{10}Cd_2Sb_4S_{13}$, and $Cu_{10}Fe_2Sb_4S_{13}$ phases are the ones with the lowest levels with 456 S/m, 443 S/m, and 394 S/m, respectively. The results agree with other thermoelectric materials studied and are synthesized with fast techniques such as the mechanical milling [29]. This behavior is possibly because the flow of electric current is hampered by encountering dislocations caused by mechanical grinding. However, the substitution by other elements increases the Seebeck coefficient and decreases the thermal conductivity, which is beneficial to increasing the figure of merit. The higher the value obtained for conductivity, the greater the number of positive charges.
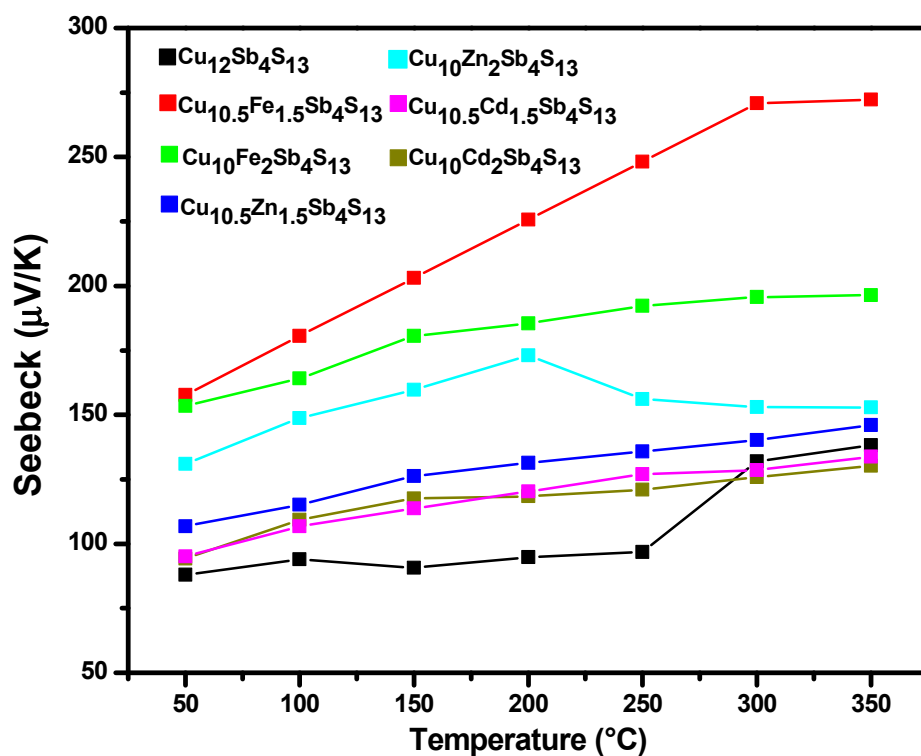
Figure 5. Seebeck coefficient for the tetrahedrite phase without substitution and for the mono-substituted tetrahedrites.
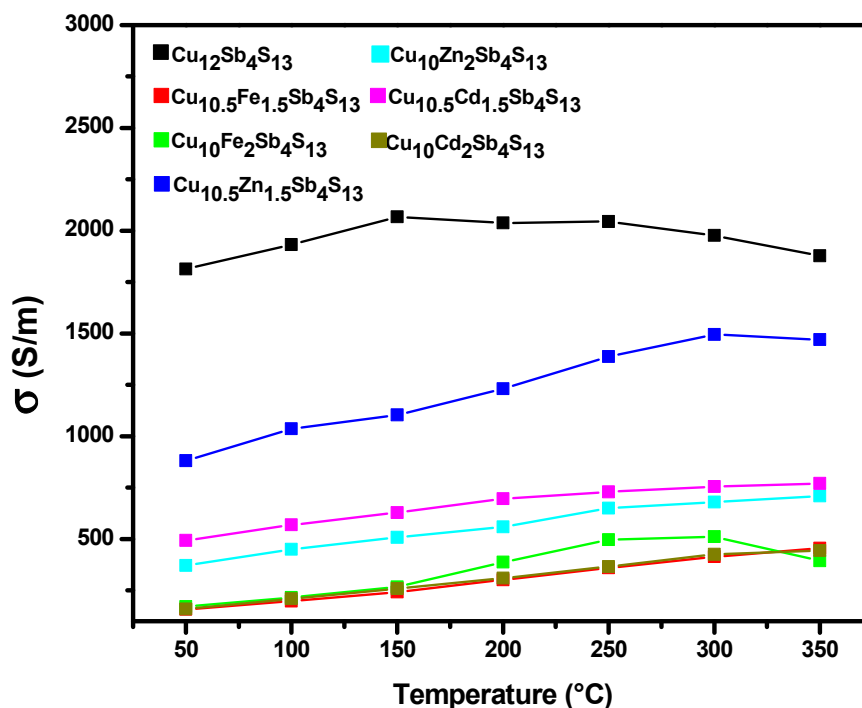

Figure 6. Electrical conductivity in pristine tetrahedrite and in mono-substituted $Cu_{12-x}M_xSb_4S_{13}$ (M = Cd, Fe, Zn) in a temperature range between 50 and 350 °C.

With the results of the thermal and electrical properties, it is possible to obtain the figure of merit for each compound. Figure 7 shows the zT values for the analyzed mono-substituted samples as well as the base tetrahedrite. The materials with formula $Cu_{12-x}M_xSb_4S_{13}$ that present the highest zT values are $Cu_{10.5}Fe_{1.5}Sb_4S_{13}$ with zT = 0.057,

followed by $Cu_{10.5}Zn_{1.5}Sb_4S_{13}$ zT = 0.048. The first one has a low electrical conductivity of 456 S/m; however, its Seebeck coefficient is the highest (7.41×10^{-8}), while the second one has the highest electrical conductivity of the substituted samples with 1470 S/m. Tetrahedrite in its base form has a zT = 0.035 despite its poor thermal properties; however, it is the sample that presents the highest electrical conductivity results with 1877 S/m. zT values obtained for tetrahedrite-based samples vary widely depending on factors such as the synthesis and sintering conditions, dopant, and doping levels; furthermore, samples having theoretically a similar chemical composition but obtained by different research groups using similar procedures yield different zT values. Thus, values reported for pristine $Cu_{12}Sb_4S_{13}$ include 0.13 at 400 K [30], 0.52 at 600 K [31], 0.76 at 623 K [27], or 0.65 at 723 K [32]. According to the literature, zT values for Fe-doped tetrahedrites, $Cu_{12-x}Fe_xSb_4S_{13}$, are very sensible to Fe content and temperature, with the highest values obtained when $x \leq 1$ and the temperature higher than 700 K. Thus, some reported values are 0.01 (at 340 K), 0.6 (550 K), and 0.8 (720 K) measured for respectively, $Cu_{10}Fe_2Sb_4S_{13}$ [33], $Cu_{11}FeSb_4S_{13}$ [34], and $Cu_{11.5}Fe_{0.5}Sb_4S_{13}$ [35]. Zn-doped tetrahedrites have been also studied, yielding zT values of 0.03 at 340 K [33], 0.038 at 573 K [36], or even 1.0 at 723 K [35]. As for Cd-doping, zT values as high as 0.9 at 623 K have been reported for $Cu_{11.25}Cd_{0.75}Sb_4S_{13}$ [27]. In general, the values found in this study are lower than those mentioned above. Slight compositional changes, undetected secondary phases, and residual porosity might account for some of these discrepancies. The results of density, diffusivity, and thermal and electrical conductivity measurements to obtain the figure of merit of each material from this work are listed in Table 3.
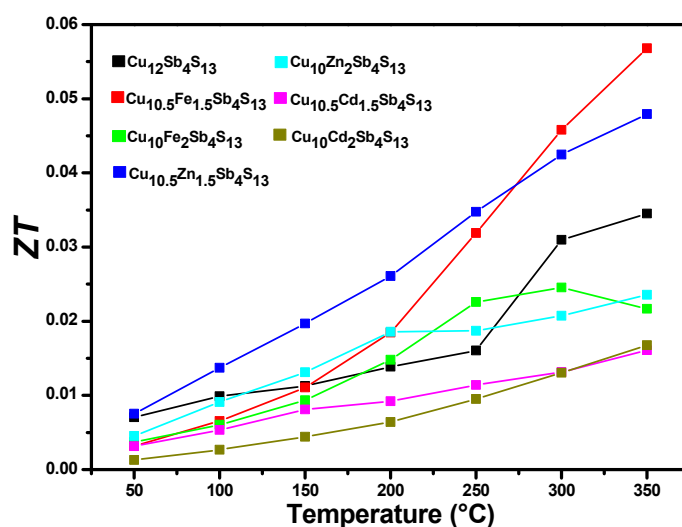

Figure 7. Figure of merit of pristine tetrahedrite and the substituted $Cu_{12-x}M_xSb_4S_{13}$-type tetrahedrite family.

Table 3. Results corresponding to the parameters of thermal and electrical conductivity to obtain the figure of merit.

	Tetrahedrites	ρ (kg/m³)	α (m²/s)	κ (W/m K)	S (μV/K)	σ (S)	zT
Pristine	$Cu_{12}Sb_4S_{13}$	4662.162	2.69×10^{-7}	0.647	1.91×10^{-8}	1876.89	0.035
Mono-substituted	$Cu_{10}Fe_{1.5}Cu_{0.5}Sb_4S_{13}$	4333.333	1.63×10^{-7}	0.370	7.41×10^{-8}	455.52	0.057
	$Cu_{10}Fe_2Sb_4S_{13}$	4283.582	1.80×10^{-7}	0.437	3.86×10^{-8}	394.32	0.022
	$Cu_{10}Zn_{1.5}Cu_{0.5}Sb_4S_{13}$	4127.45	1.80×10^{-7}	0.408	2.13×10^{-8}	1469.59	0.048
	$Cu_{10}Zn_2Sb_4S_{13}$	4342.857	1.93×10^{-7}	0.438	2.34×10^{-8}	708.66	0.024
	$Cu_{10}Cd_{1.5}Cu_{0.5}Sb_4S_{13}$	4255.319	2.13×10^{-7}	0.507	1.70×10^{-8}	769.99	0.016
	$Cu_{10}Cd_2Sb_4S_{13}$	4448.275	1.34×10^{-7}	0.295	1.79×10^{-8}	443.26	0.017

4. Conclusions

It is possible to obtain $Cu_{12}Sb_4S_{13}$-type materials by mechanical grinding as well as the partial or total substitution of covellite in the tetrahedrite phase without the need for the use of inert atmospheres employing short synthesis times starting from a mixture of high-purity commercial reagents. This also showed that the electrical and thermal properties obtained are similar or even bigger than those reported for thermoelectric materials in this temperature range.

Author Contributions: Conceptualization: F.A.L.C., J.A.D.-G. and A.F.F.; methodology: F.A.L.C., J.A.D.-G. and A.F.F. (synthesis), F.A.L.C. and J.R.-H. (Rietveld analysis); F.A.L.C., O.J.D. and M.A.L.d.l.T. (electrical and thermal measurements); writing—original draft preparation: F.A.L.C. and A.F.F.; writing—review and editing: all authors.. All authors have read and agreed to the published version of the manuscript.

Institutional Review Board Statement: Not applicable.

Informed Consent Statement: Not applicable.

Data Availability Statement: These results are part of F.A.L.C. Ph.D. project carried out at Cinvestav del IPN, Unidad Saltillo, Mexico.

Conflicts of Interest: The authors declare no conflict of interest.

References

1. Morris, A.S.; Langari, R. Temperature measurement. In *Measurement and Instrumentation: Theory and Applications, Chapter 14*; Academy Press: San Diego, CA, USA, 2012; pp. 347–392. ISBN 978-0-12-381960-4.
2. Janak, L.; Ancik, Z.; Vestika, J.; Hadas, Z. Thermoelectric Generator Based on MEMS Module as an Electric Powe Backup in Aerospace Applications. *Mater. Today Proc.* **2015**, *2*, 865–870. [CrossRef]
3. Mahan, G.D.; Sofo, J.O. The best thermoelectric. *Proc. Natl. Acad. Sci. USA* **1996**, *93*, 7436–7439. [CrossRef] [PubMed]
4. Kishan, K.Y.; Bisht, N.; Hiragond, C.; Dey, A.; Khanna, P.K.; More, P.V. Room temperature thermoelectric performance of Methyl Ammonium Lead Iodide Perovskite and their MWCNT-PANI composites. *Mater. Today Chem.* **2020**, *17*, 100275. [CrossRef]
5. Harizanova, S.G.; Zhecheva, E.N.; Valchev, V.D.; Khristov, M.G.; Stoyanova, R.K. Improving the thermoelectric efficiency of Co based ceramics. *Mater. Today Proc.* **2015**, *2*, 4256–4261. [CrossRef]
6. Ramasamy, K.; Gupta, R.K.; Palchoudhury, S.; Ivanov, S.; Gupta, A. Layer-Structured Copper Antimony Chalcogenides ($CuSbSe_xS_{2-x}$): Stable Electrode Materials for Supercapacitors. *Chem. Mater.* **2015**, *27*, 379–386. [CrossRef]
7. Wu, Y.; Finefrock, S.W.; Yang, H. Nanostructured thermoelectric: Opportunities and challenges. *Nano Energy* **2012**, *1*, 651–653. [CrossRef]
8. Zhao, D.; Tan, G. A review of thermoelectric cooling: Materials, modeling and applications. *Appl. Therm. Eng.* **2014**, *66*, 15–24. [CrossRef]
9. Vanalakar, S.A.; Agawane, G.L.; Shin, S.W.; Yang, H.S.; Patil, P.S.; Kim, J.Y.; Kim, J.H. Non-vacuum mechanochemical route to the synthesis of Cu_2SnS_3 nano-ink for solar cell applications. *Acta Mater.* **2015**, *85*, 314–321. [CrossRef]
10. Su, H.; Xie, Y.; Wan, S.; Bin, B.; Qian, Y. A novel one-step solvothermal route to nanocrystalline $CuSbS_2$ and Ag_3SbS_3. *Solid State Ion.* **1999**, *123*, 319–324. [CrossRef]
11. Zou, Y.; Jiang, J. Colloidal synthesis of chalcostibite copper antimony sulfide nanocrystals. *Mater. Lett.* **2014**, *123*, 66–69. [CrossRef]
12. Zhang, Y.; Qiao, Z.; Chen, X. Microwave-Assisted Elemental-Direct-Reaction route to Nanocrystalline Copper sulfides Cu_9S_8 and Cu_7S_6. *J. Solid Satate Chem.* **2002**, *253*, 249–253. [CrossRef]
13. Baláž, P.; Baláž, M.; Achimovičová, M.; Bujňáková, Z.; Dutková, E. Chalcogenide mechanochemistry in materials science: Insight into synthesis and applications (a review). *J. Mater. Sci.* **2017**, *52*, 11851–11890. [CrossRef]
14. Baláž, M.; Zorkovská, A.; Urakaev, F.; Baláž, P.; Briančin, J.; Bujňáková, Z.; Achimovičová, M.; Gock, E. Ultrafast mechanochemical synthesis of copper sulfides. *RSC Adv.* **2016**, *6*, 87836–87842. [CrossRef]
15. Baláž, P.; Guilmeau, E.; Daneau, N.; Dobrozhan, O.; Baláž, M.; Hegedus, M.; Barbier, T.; Achimovicová, M.; Briancin, J. Tetrahedrites synthesized via scalable mechanochemical process and spark plasma sintering. *J. Eur. Ceram. Soc.* **2020**, *40*, 1922–1930. [CrossRef]
16. Barbier, T.; Rollin-Martinet, S.; Lemoine, P.; Gascoin, F.; Kaltzolou, A.; Vaqueiro, P.; Powell, A.V.; Guikmeau, E. Thermoelectric Material: A New Rapid Synthesis Process for Nontoxic and High-Performance Tetrahedrite Compound. *J. Am. Ceram. Soc.* **2015**, *6*, 36801. [CrossRef]
17. Suryanarayana, C. Mechanical alloying and milling. *Prog. Mater. Sci.* **2001**, *46*, 1–84.

18. Lu, X.; Morelli, D.T. Rapid synthesis of high-performance thermoelectric materials directly from natural mineral tetrahedrite. *MRS Commun.* **2013**, *3*, 129–133. [CrossRef]

19. Rodríguez-Carvajal, J. Recent advances in magnetic structure determination by neutron powder diffraction. *Phys. B* **1993**, *192*, 55–69. [CrossRef]

20. Le Bail, A. Whole powder pattern decomposition methods and applications: A retrospection. *Powder Diffr.* **2005**, *20*, 316–326. [CrossRef]

21. *NIST Inorganic Crystal Structure Database, 2012 Version*; National Institute of Standards and Technology: Gaithersburg, MD, USA, 2012.

22. Makovicky, E. Crystal structures of sulfides and other chalcogenides. *Rev. Miner. Geochem.* **2006**, *61*, 7–125. [CrossRef]

23. Chetty, R.; Bali, A.; Mallik, R.C. Tetrahedrites as thermoelectric materials: An overview. *J. Mater. Chem.* **2015**, *3*, 12364–12378. [CrossRef]

24. Chen, K.; Zhou, J.; Chen, W.; Chen, Q.; Zhou, P.; Liu, Y. A green synthesis route for the phase and size tunability of copper antimony sulfide. *Nanoscale* **2016**, *8*, 5146–5152. [CrossRef]

25. Gonzales, A.P.; Lopes, E.B.; Villeroy, B.; Monnier, J.; Godart, C.; Lenoir, B. Effect of Ni, Bi and Se on the tetrahedrite formation. *RSC Adv.* **2016**, *6*, 102359–102367.

26. Goto, Y.; Sakai, Y.; Kamihara, Y.; Matoba, M. Effect of Sn-Substitution on Thermoelectric Properties of Copper-Based sulfide, Famatinite Cu_3SbS_4. *J. Phys. Soc. Jpn.* **2015**, *84*, 2015. [CrossRef]

27. Kumar, D.S.P.; Chetty, R.; Rogl, P.; Rogl, G.; Baer, E.; Malar, P.; Mallik, R.C. Thermoelectric properties of Cd doped tetrahedrite: $Cu_{12-x}CdxSb_4S_{13}$. *Intermetallics* **2016**, *78*, 21–29. [CrossRef]

28. Levinsky, P.; Vaney, J.B.; Candolfi, C.; Dauscher, A.; Lenoir, B.; Hejtmanek, J. Electrical, Thermal, and Magnetic Characterization of Natural Tetrahedrites-Tennantites of Different Origin. *J. Electron. Mater.* **2015**, *45*, 1351–1357. [CrossRef]

29. Weller, D.P.; Morelli, D.T. Rapid synthesis of zinc and nickel co-doped tetrahedrite thermoelectrics by reactive spark plasma sintering and mechanical alloying. *J. Alloys Compd.* **2017**, *710*, 794–799. [CrossRef]

30. Nasonova, D.; Verchenko VYu Tsirlin, A.A.; Shevelkov, A.V. Low temperature structure and thermoelectric properties of pristine tetrahedrite $Cu_{12}Sb_4S_{13}$. *Chem. Mater.* **2016**, *28*, 6621–6627. [CrossRef]

31. Wang, J.; Gu, M.; Bao, Y.; Li, X.; Chen, L. Quick fabrication and thermoelectric properties of tetrahedrite. *J. Electron. Mater.* **2016**, *45*, 2274–2277. [CrossRef]

32. Sun, F.-H.; Wu, C.-F.; Li, Z.; Pan, Y.; Asfandiyar Dong, J.; Li, J.-F. Powder metallurgically synthesized tetrahedrites: Phase transition and high thermoelectricity. *RSC Adv.* **2017**, *7*, 18909–18916. [CrossRef]

33. Suekuni, K.; Tsuruta, K.; Ariga, T.; Koyano, M. Thermoelectric properties of mineral tetrahedrites $Cu_{10}Tr_2Sb_4S_{13}$ with low thermal conductivity. *Appl. Phys. Express* **2012**, *5*, 051201. [CrossRef]

34. Guler, A.; Ballikaya, S.; Boyraz, C.; Okay, C.; Shulgin, D.; Rameev, B. Thermoelectric properties and EPR analysis of Fe doped $Cu_{12}Sb_4S_{13}$. *J. Solid State Chem.* **2019**, *269*, 547–552. [CrossRef]

35. Lu, X.; Morelli, D.T.; Xia, Y.; Zhou, F.; Ozolins, V.; Chi, H.; Zhou, X.; Uher, C. High performance thermoelectricity in earth-abundant compounds based on natural mineral tetrahedrites. *Adv. Energy Mater.* **2013**, *3*, 342–348. [CrossRef]

36. Harish, S.; Sivaprahasam, D.; Battabyal, M.; Gopalan, R. Phase stability and thermoelectric properties of $Cu_{10.5}Zn_{1.5}Sb_4S_{13}$ tetrahedrite. *J. Alloys Compd.* **2016**, *667*, 323–328. [CrossRef]